Supplementary Information

Spontaneous Deposition of High-Density Pt Single Atoms on Oxides via Charge Polarization between Oxides and Carbon

Jing-Fang Huang,*[a] Liang-Jhu Chen,[a] Bo-Zhao Yang,[a] and Jeng-Lung Chen[b]

[a] Department of Chemistry, National Chung Hsing University, Taichung 402, Taiwan

[b] National Synchrotron Radiation Research Center, Science-Based Industrial Park, Hsinchu 30076, Taiwan

Correspondence to: jfh@dragon.nchu.edu.tw

This PDF file includes:

Scheme S1

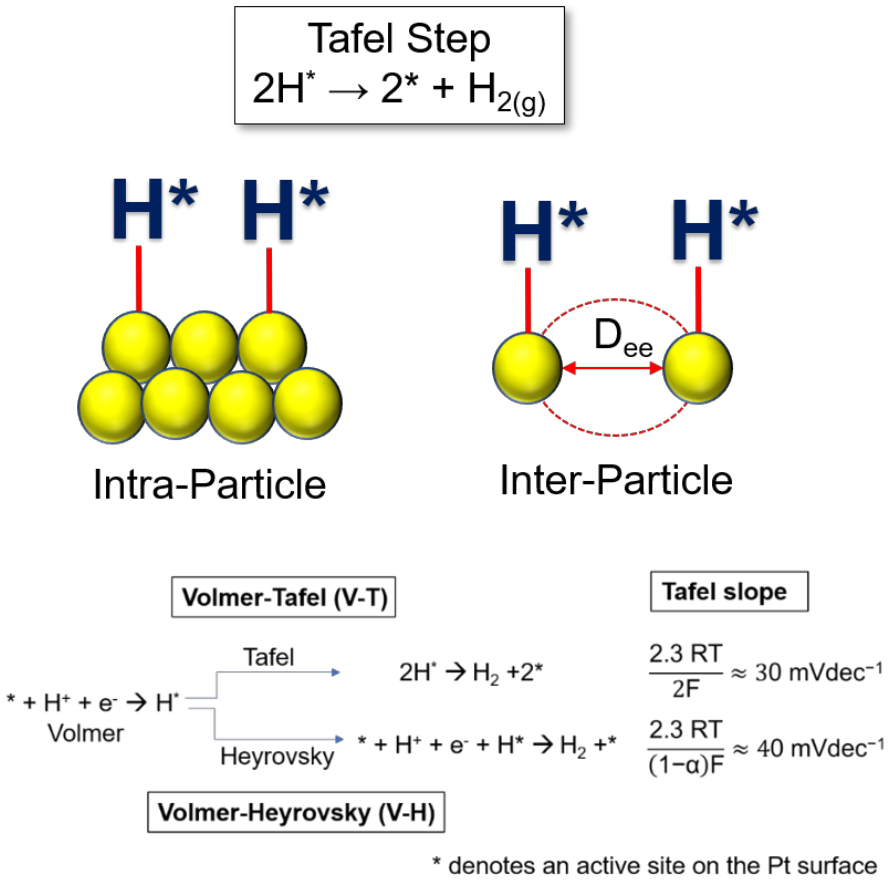

Scheme S1 D_{ee} determines the bond formation between two H*, and the HER mechanism.

Electrochemical characterization of Pt_1. The anodic charge (Q_{Pt}) of the anodic stripping of Pt_1 from the Pt_1/oxide/C/GCE was evaluated by anodic CV scanning. The Pt_1 content obtained by ICP-MS was used to confirm Q_{Pt}. A combination of $ECSA_H$ and Q_{Pt} was used to calculate the mean diameter of Pt_1 (D_{Pt1}) and the number of Pt_1s on the electrode (N_{Pt1}). Assuming that Pt_1 on the electrode is distributed uniformly and spherical in shape, $ECSA_H$ and Q_{Pt} can be calculated using Equations (1) and (2), respectively.

$$ECSA_H = \frac{\pi D_{Pt1}^{\ 2}}{2} \times N_{Pt1} \quad (1)$$

$$Q_{Pt} = \frac{\pi D_{Pt1}^{\ 3} \rho_{Pt}}{6M_{Pt}} \times n \times F \times N_{Pt1} \quad (2)$$

where n= 4 is the number of electrons transferred for the anodic stripping of Pt, F is the Faraday constant, ρ_{Pt} is the density of Pt (21.09 g cm^{-3}), and M_{Pt} is the atomic mass of Pt. The $Q_{Pt1}/ECSA_H$ ratio for evaluating the D_{Pt1} of Pt_1 is shown by Equation (3):

$$D_{Pt1} = \frac{3M_{Pt}}{4F\rho_{Pt}} \times \frac{Q_{Pt1}}{ECSA_H} \quad (3)$$

Then, N_{Pt1} can be obtained from D_{Pt1}.

Electrochemical determination of D_{ee}.

We propose the adjacent Pt_1s distance (D_{ee}, the edge-to-edge distance between two adjacent SAs) as a controlling parameter for the HER kinetics of the Pt_1-SACs. D_{ee} represents the distance between two Pt_1s affected by the control parameters (D_{Pt1}, A_{BET} (the Brunauer-Emmett-Teller (BET) surface area of oxides), and Pt loading). We assume that all Pt_1s exhibit spherical shapes for the calculation of D_{ee}. The Pt_1s are monodispersed and homogeneously distributed on the oxide support (Scheme S2).

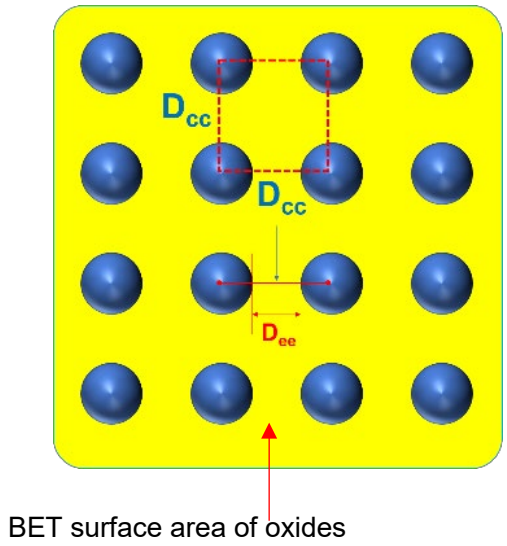

Scheme S2 Evaluation of D_{ee}: D_{cc} (center-to-center distance between Pt_1) = $(A_{BET}/N_{Pt1})^{0.5}$, D_{ee} = D_{cc}-D_{Pt1}=$(A_{BET}/N_{Pt1})^{0.5}$-D_{Pt1}. (Note: N_{Pt1} is the number of Pt_1 atoms and A_{BET} is the BET surface area of the oxide).

Figure S1

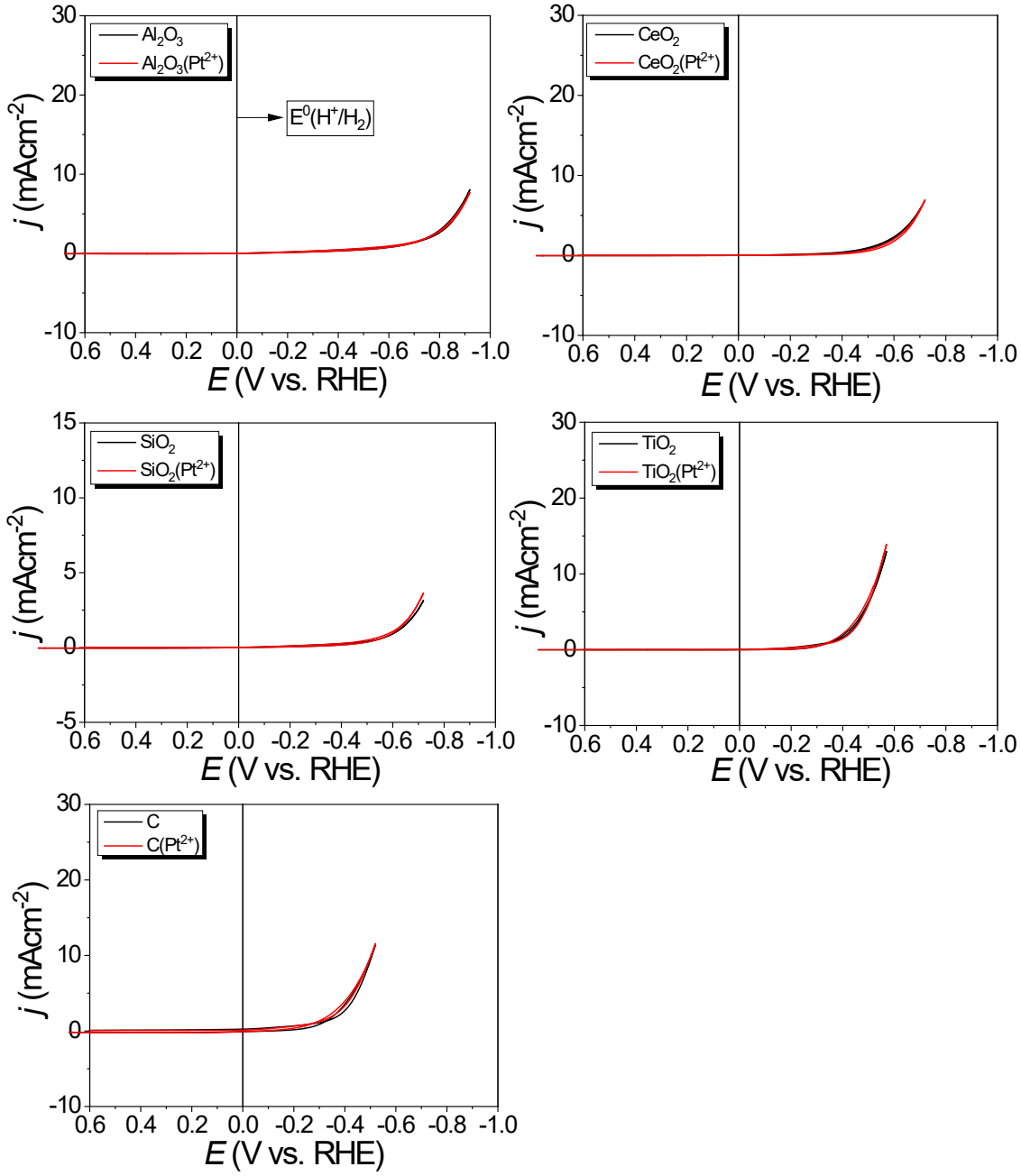

Figure S1. CVs of oxides and C before (black line) and after (red line) incubation with Pt_{aq} for 16 h in Ar-saturated 0.5 M H_2SO_4 at a scan rate of 50 mVs^{-1} .

Figure S2

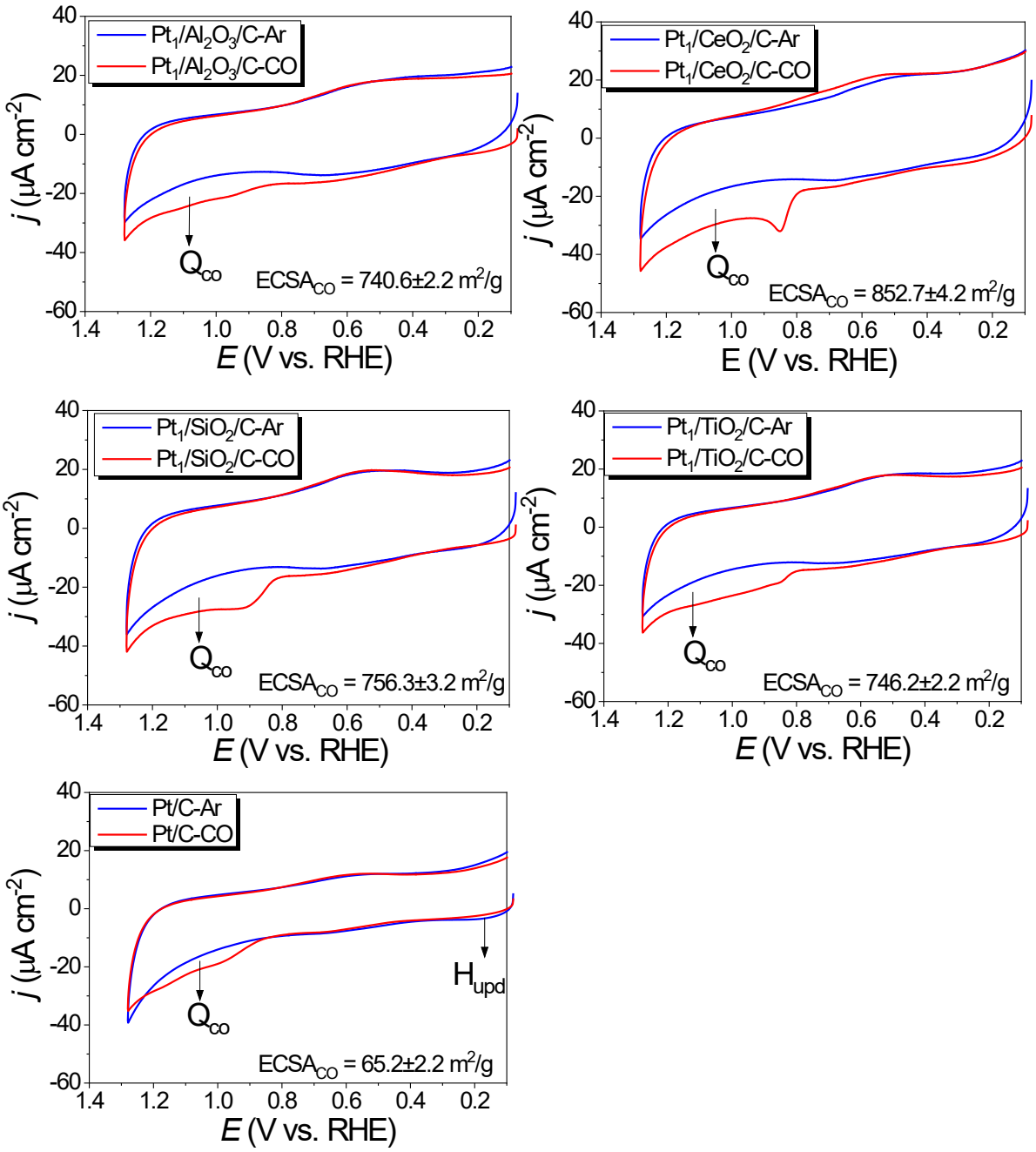

Figure S2 CVs curves of CO_s for Pt_1/oxide/C and Pt/C.

Figure S3

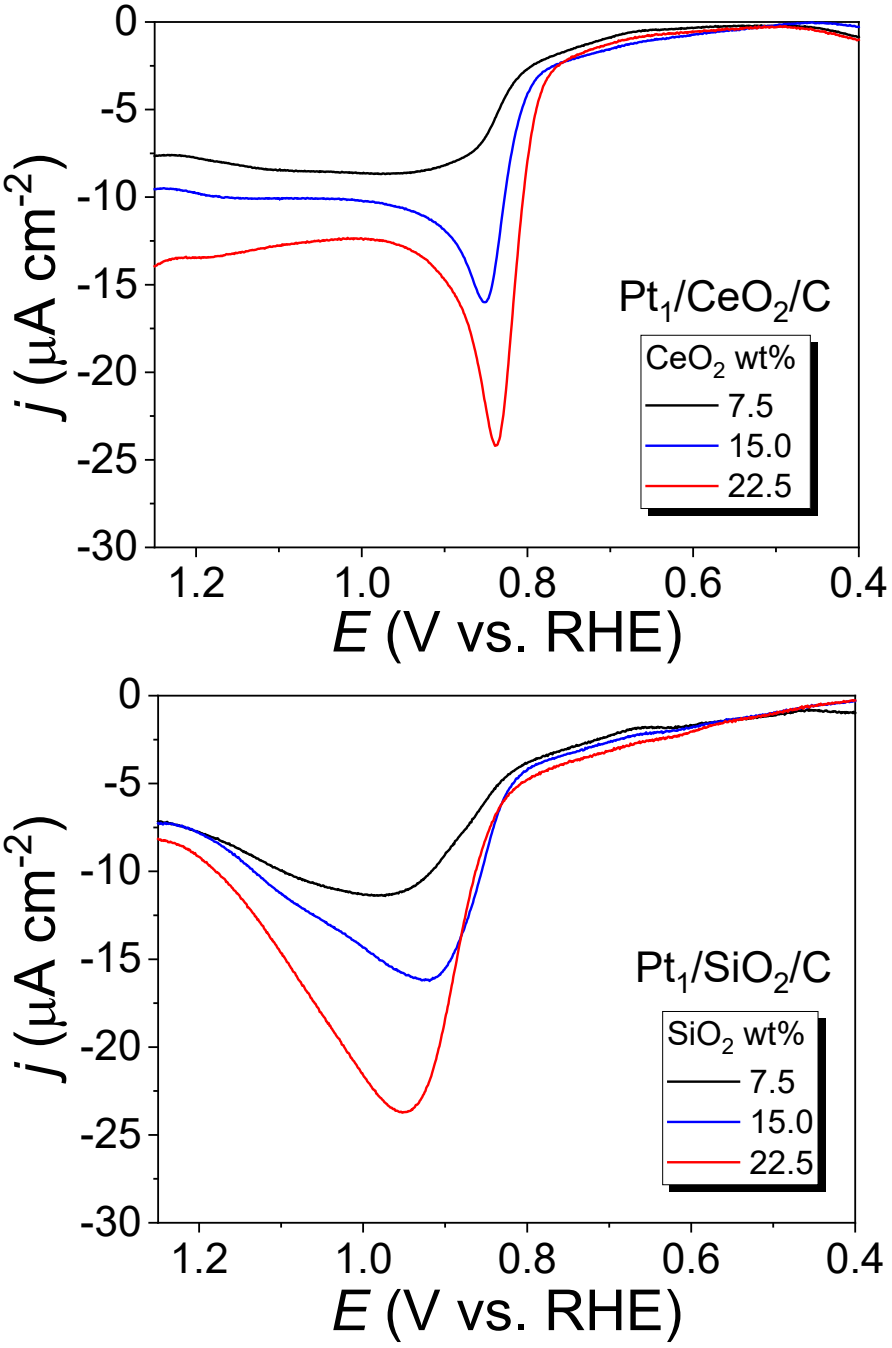

Figure S3 CO-stripping curves for Pt_1/oxide/C with various oxide contents.

Figure S4

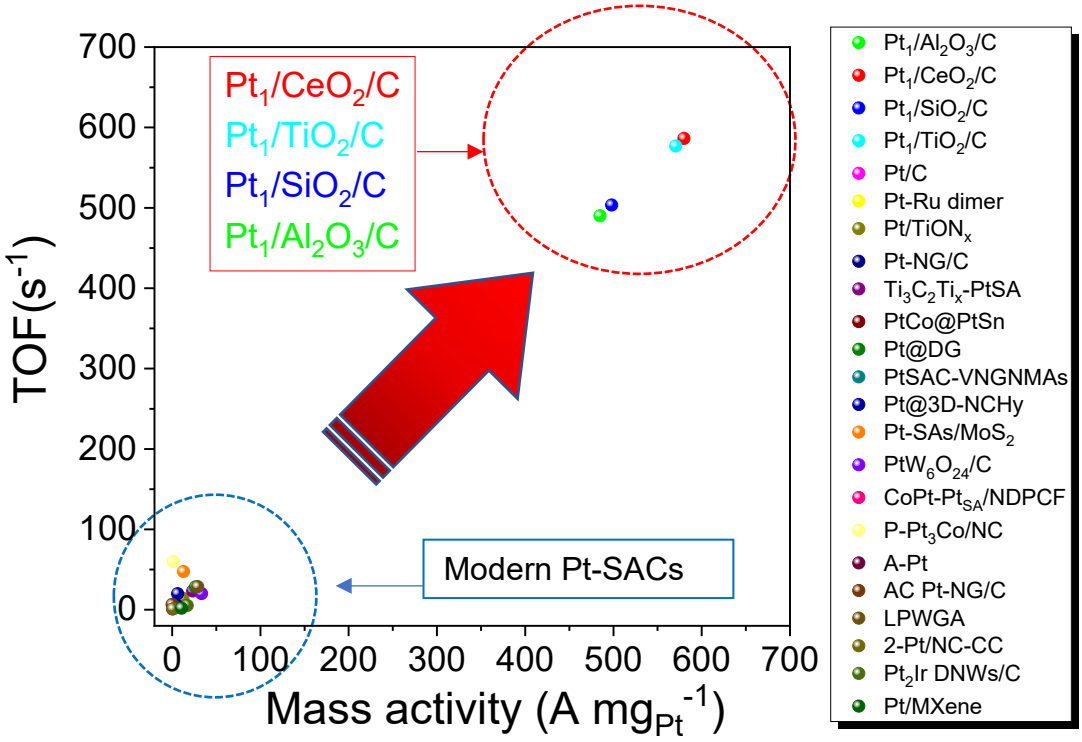

Figure S4 i_{mPt} vs. TOF for Pt_1/oxide/C and state-of-the-art Pt_1-SACs in Table S2.

Figure S5

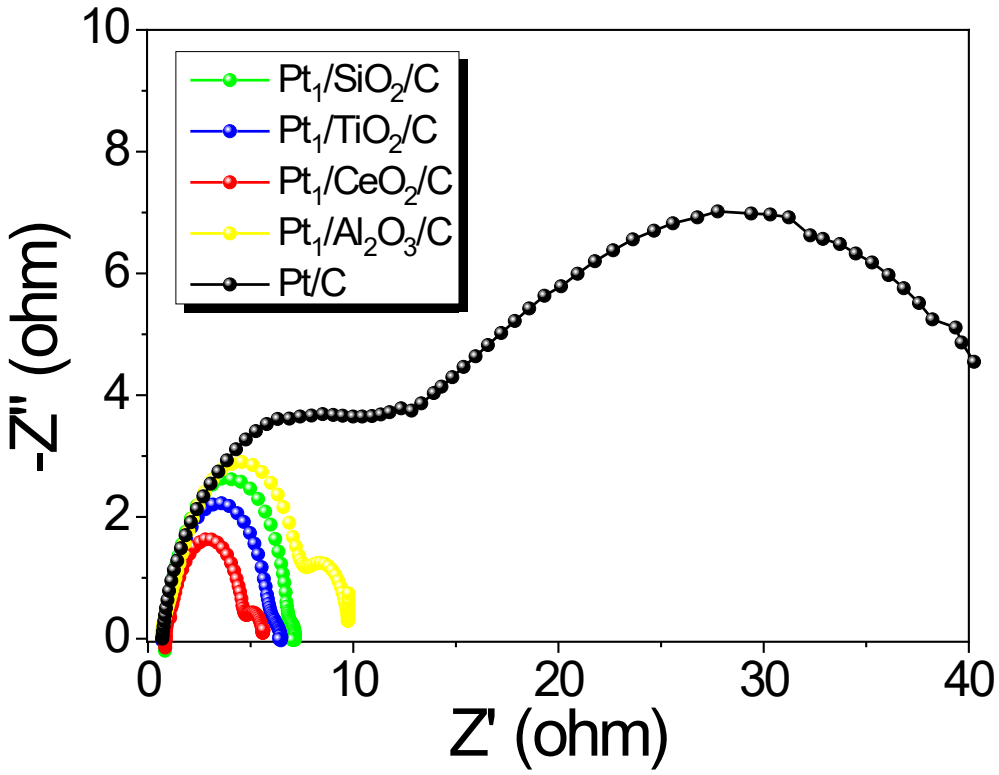

Figure S5 EIS spectra of Pt_1/oxide/C and Pt/C in Ar-purged H_2SO_4 at η = 20 mV.

Figure S6

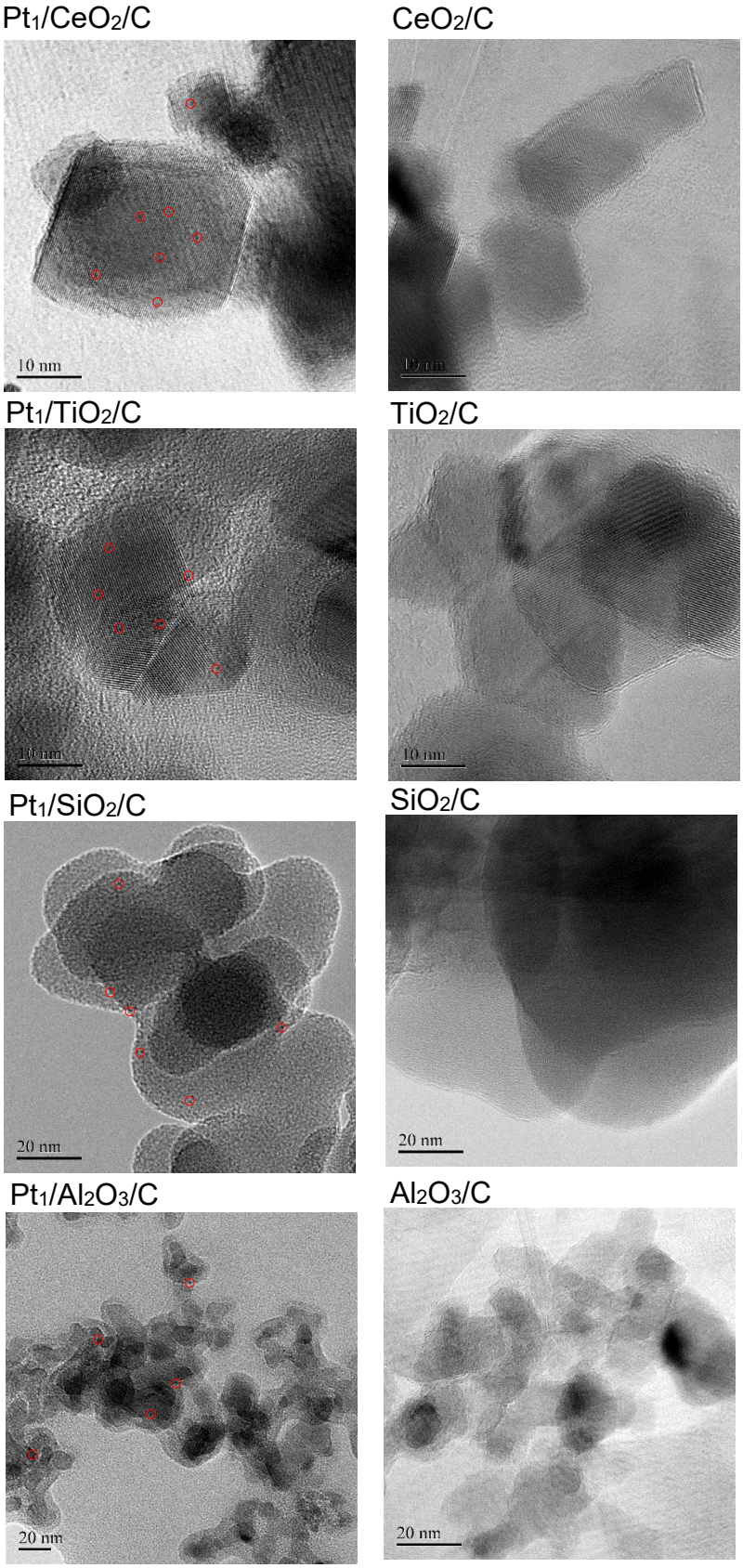

Figure S6 HR-TEM images of Pt_1/oxide/C (left) and oxide/C (right). P_1s are selectively highlighted by red circles.

Figure S7

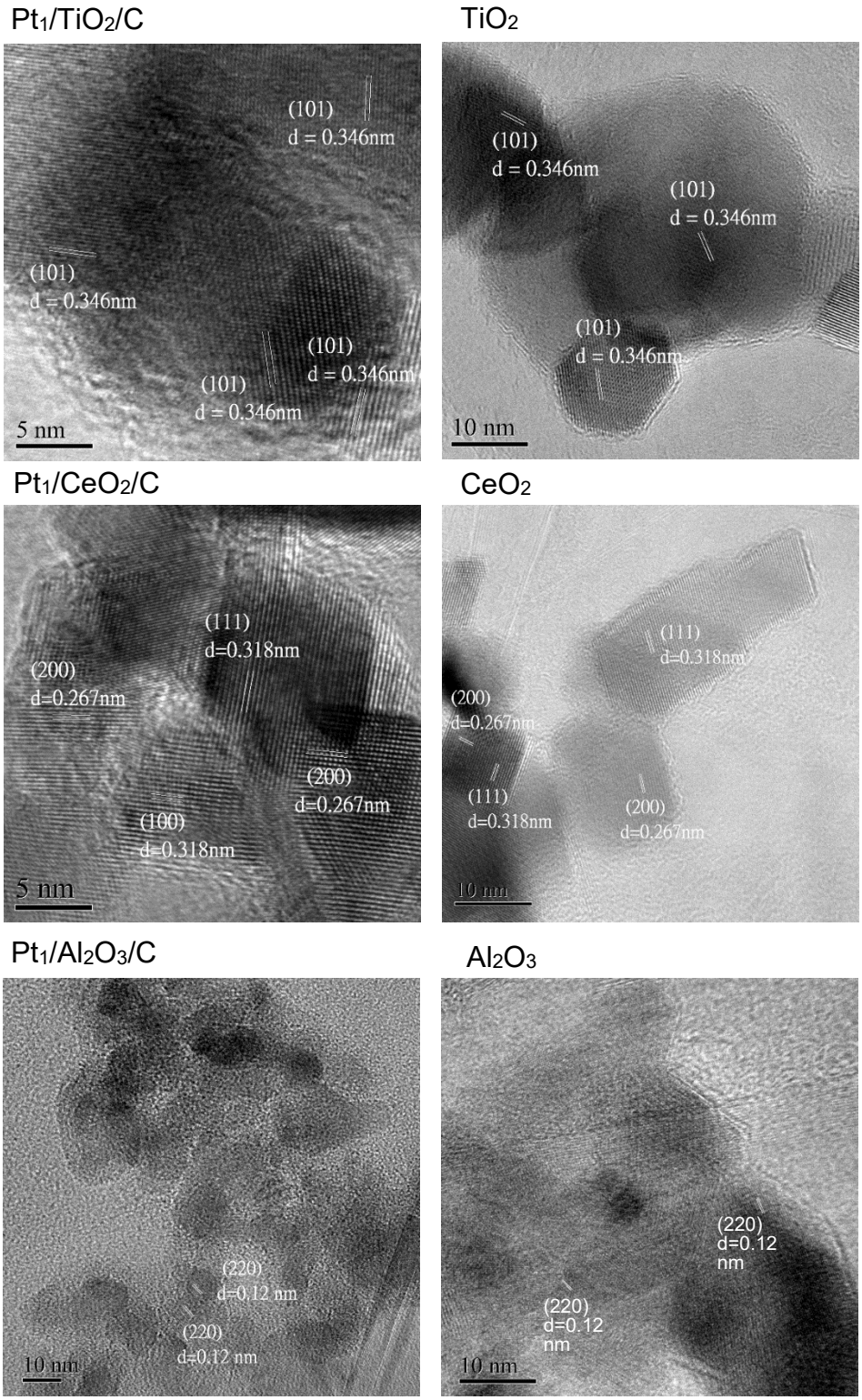

Figure S7 HR-TEM images of Pt_1/oxide/C (left) and oxide/C (right). Lattice fringes are selectively marked.

Figure S8

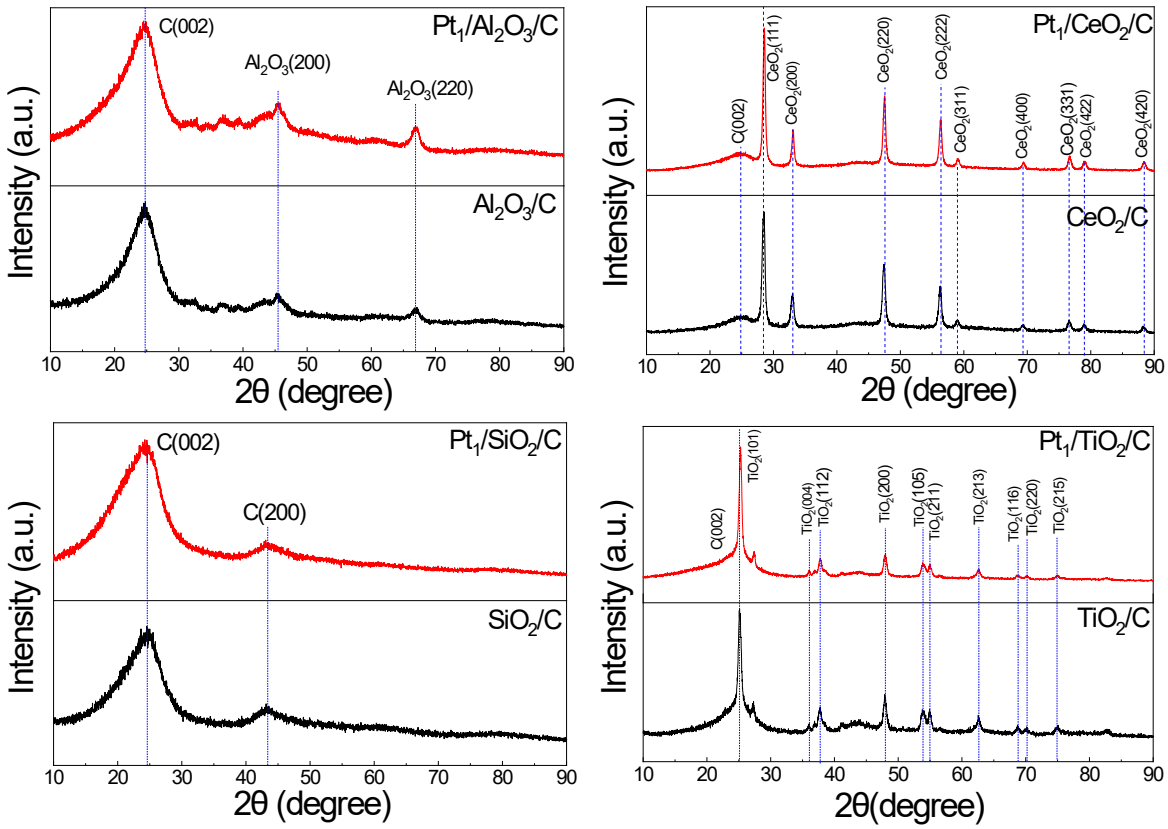

Figure S8 XRD patterns (Cu Kα) of oxide/C (black line) and Pt_1/oxide/C (red line).

Figure S9

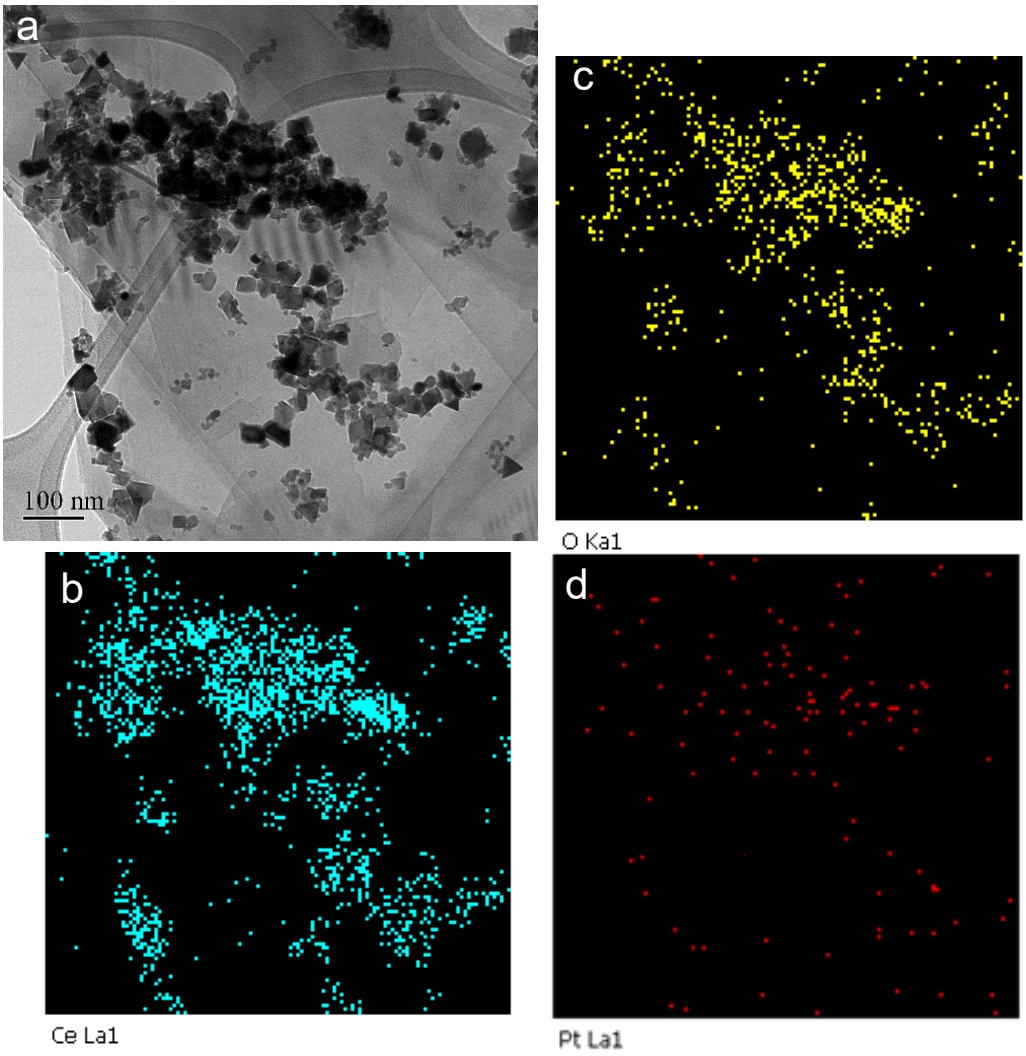

Figure S9 (a) TEM image of $Pt_1/CeO_2/C$; (b) Ce, (c) O, and (d) Pt EDS mapping in (a).

Figure S10

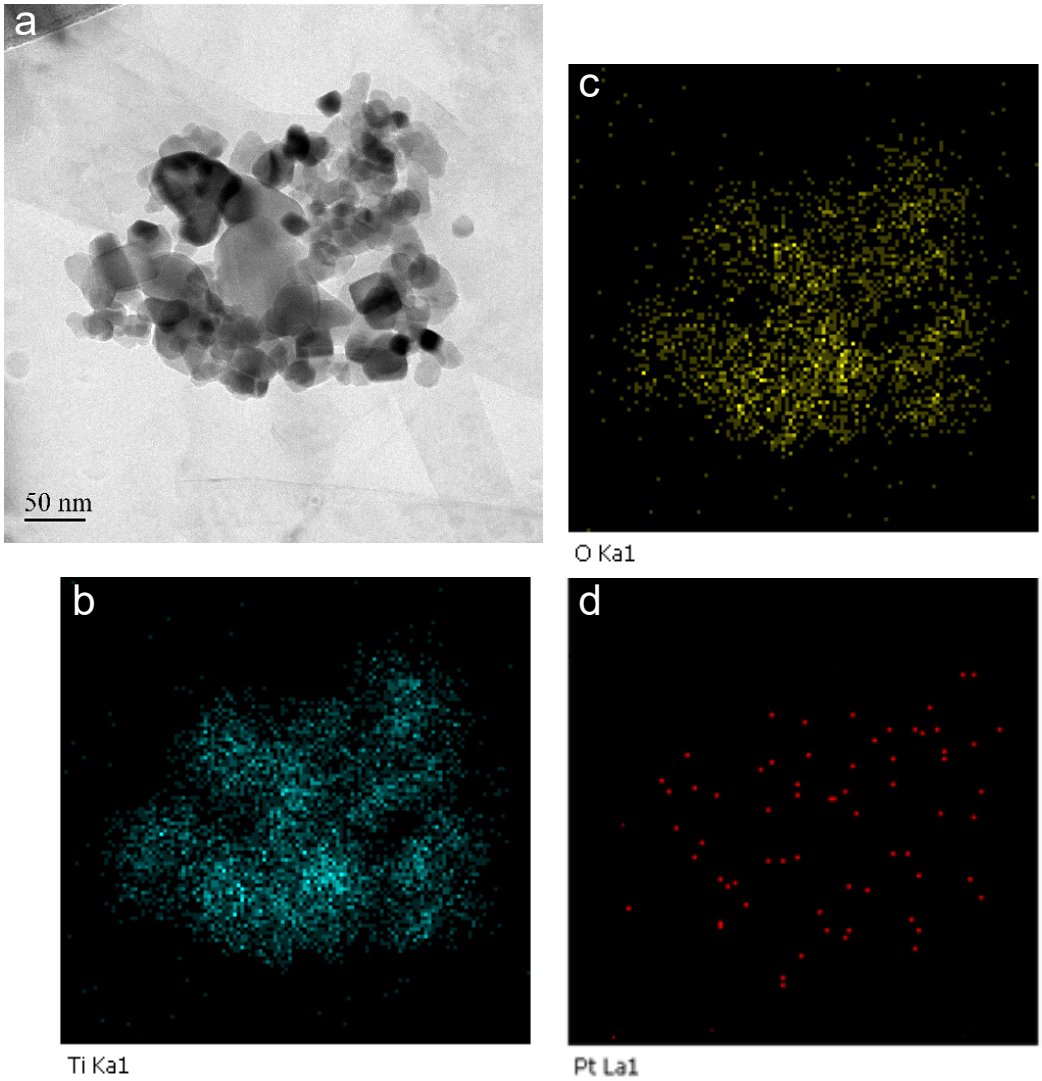

Figure S10 (a) TEM image of $Pt_1/TiO_2/C$; (b) Ti, (c) O, and (d) Pt EDS mapping in (a).

Figure S11

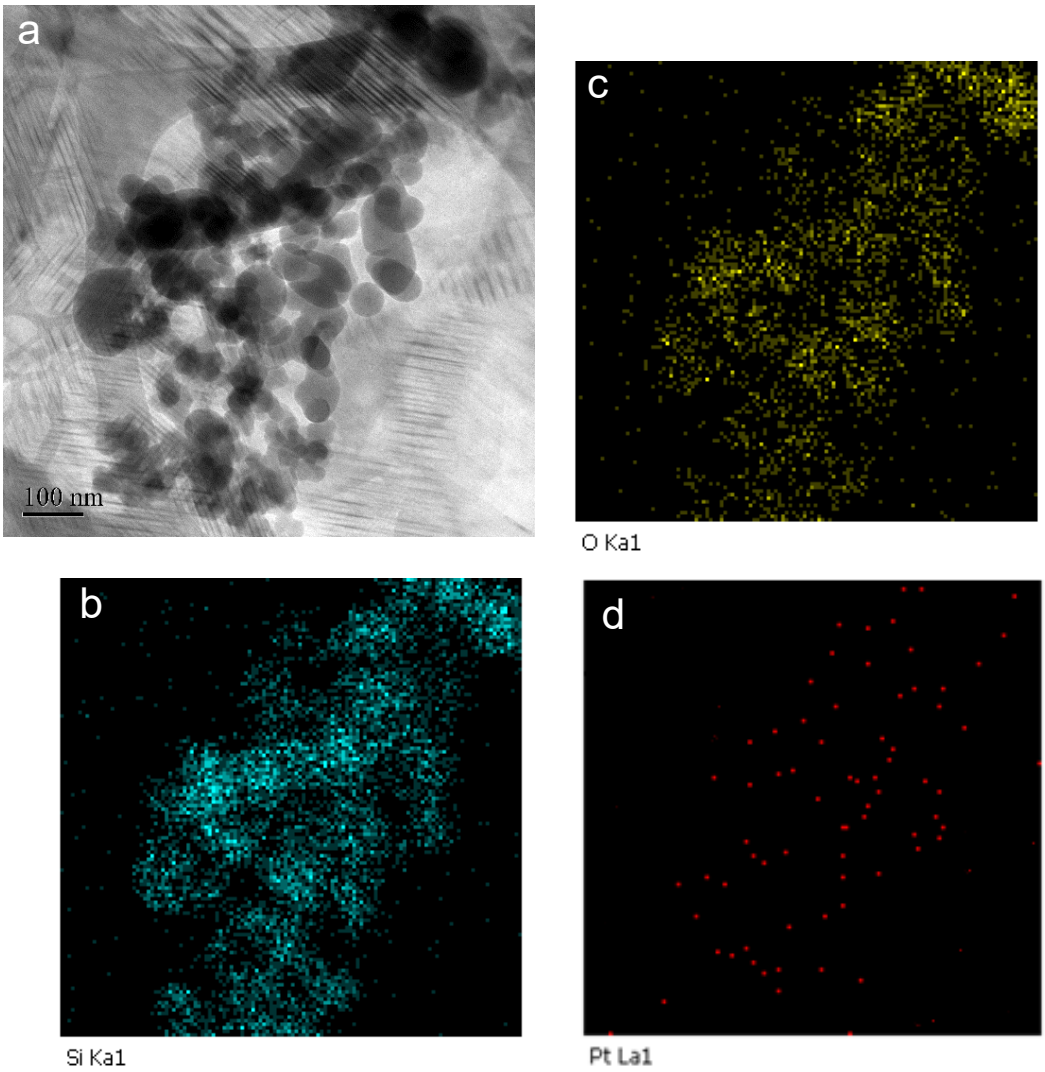

Figure S11 (a) TEM image of $Pt_1/SiO_2/C$; (b) Si, (c) O, and (d) Pt EDS mapping in (a).

Figure S12

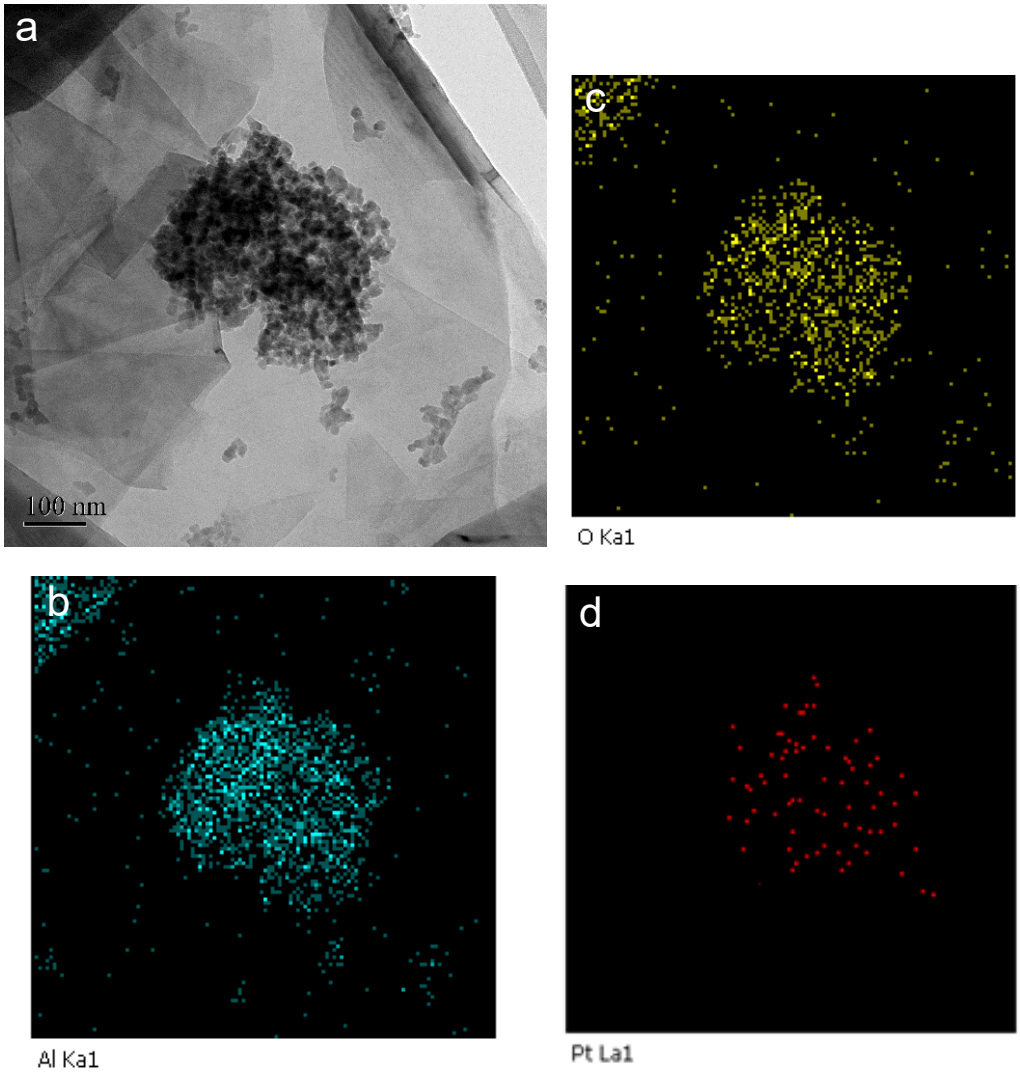

Figure S12 (a) TEM image of $Pt_1/Al_2O_3/C$; (b) Al, (c) O, and (d) Pt EDS mapping in (a).

Figure S13

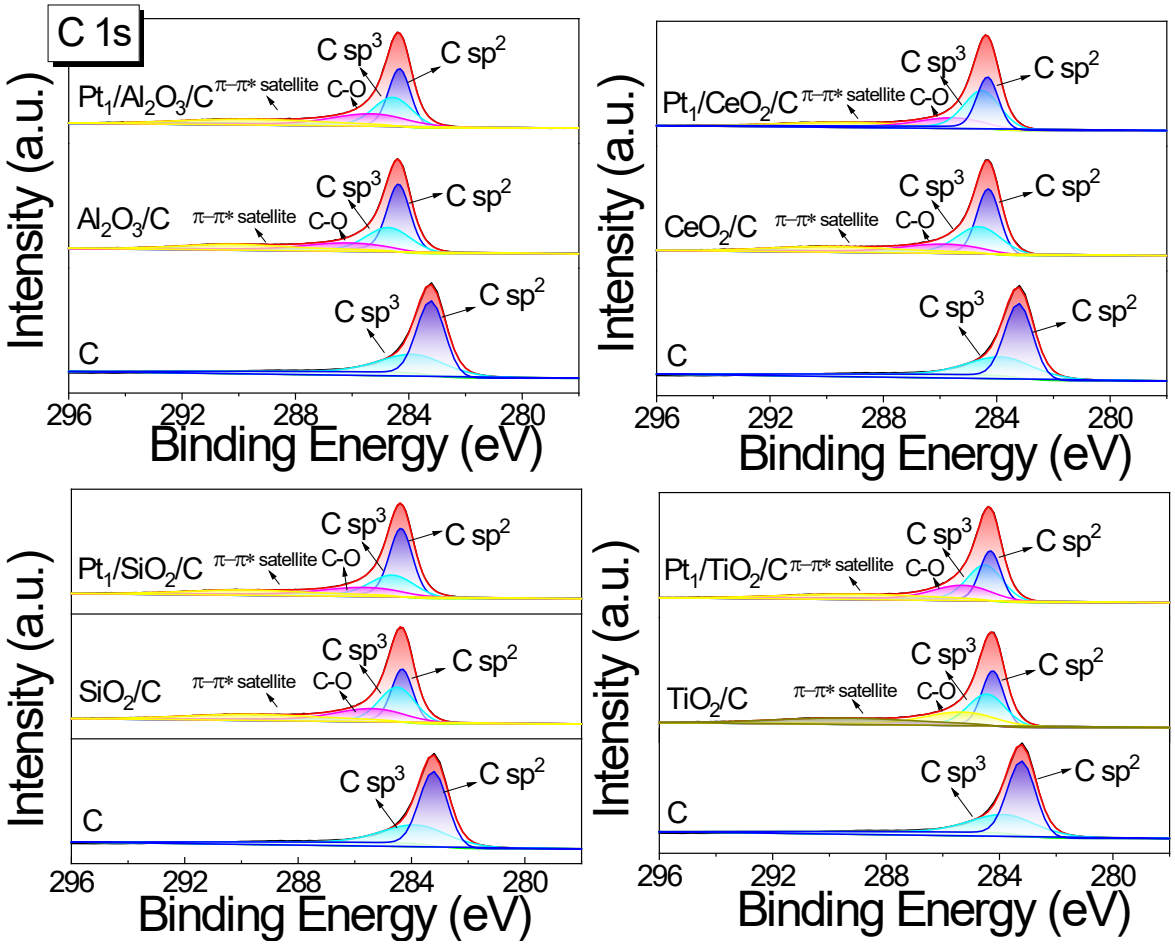

Figure S13 High-resolution XPS C 1s spectra of Pt_1/oxide/C, oxide/C, and C.

Figure S14

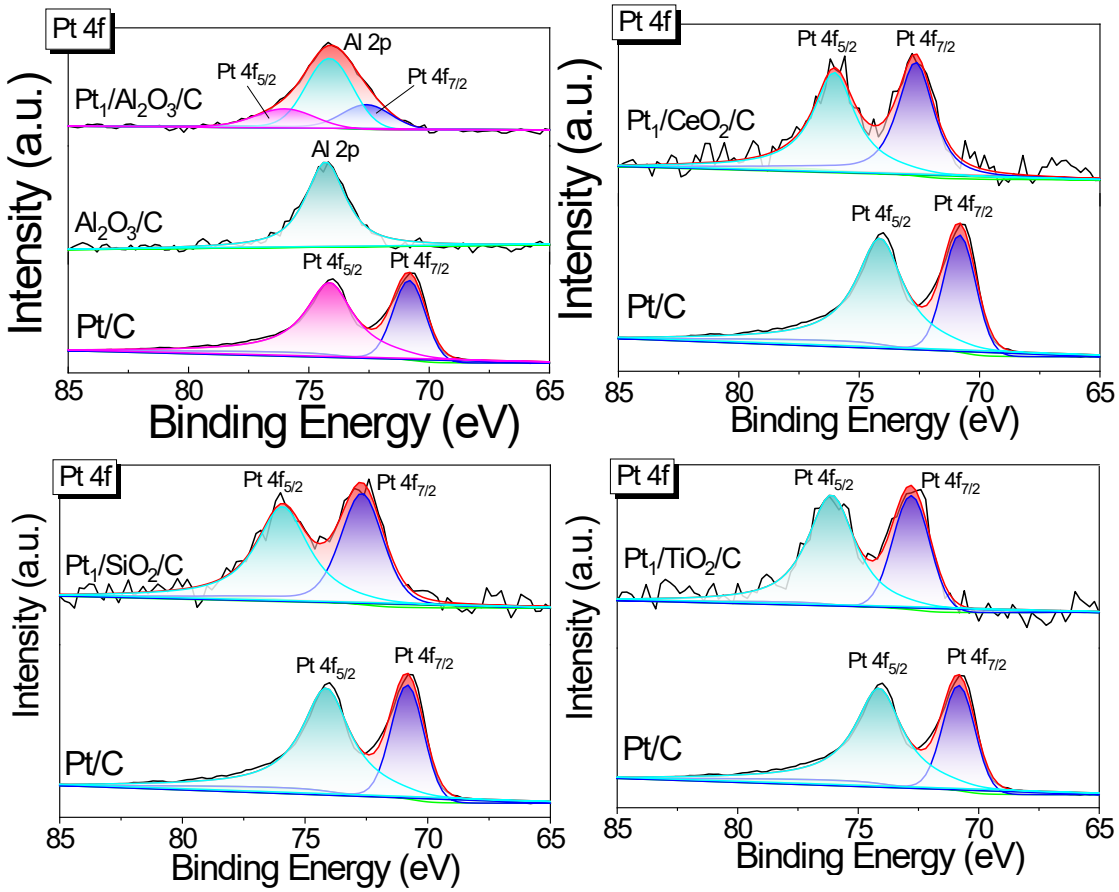

Figure S14 High-resolution XPS Pt 4f spectra of Pt_1/oxide/C and Pt/C.

Figure S15

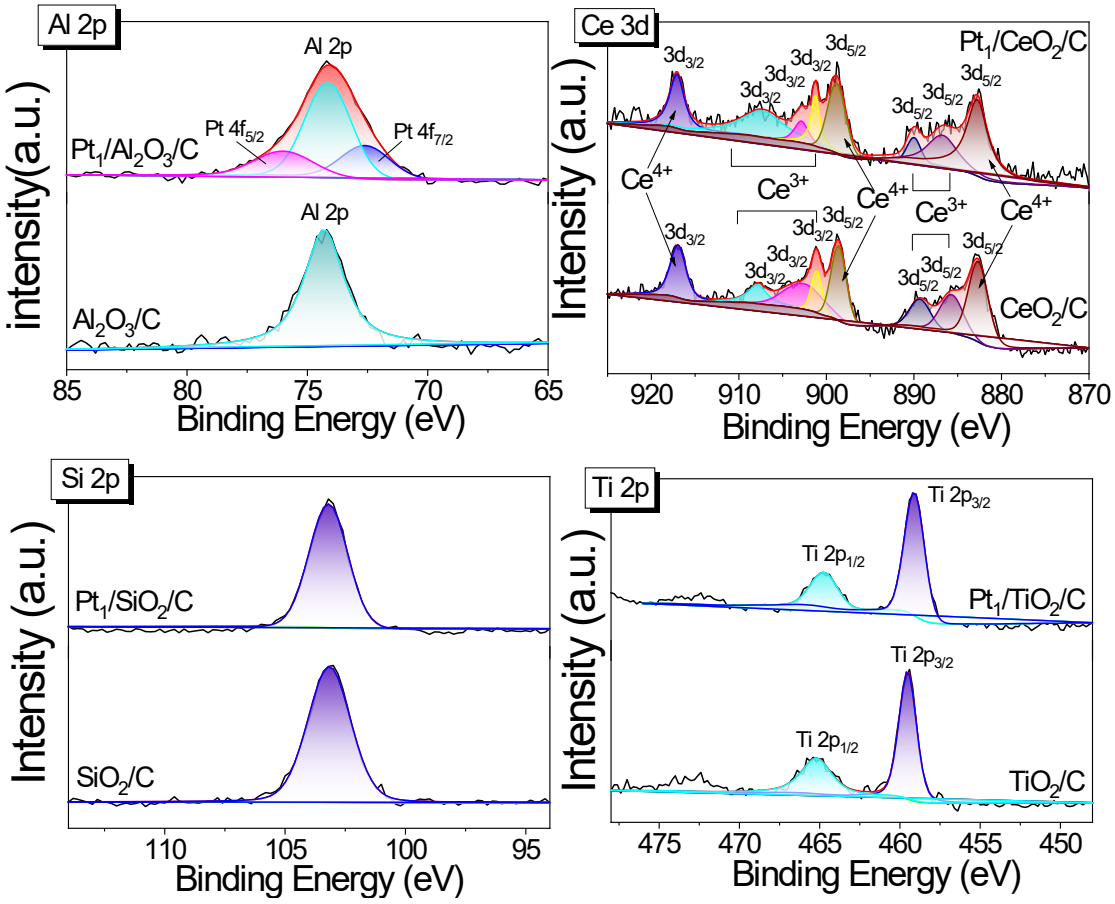

Figure S15 High-resolution XPS Al 2p, Ce 3d, Si 2p, and Ti 2p spectra of Pt_1/oxide/C and oxide/C.

Figure S16

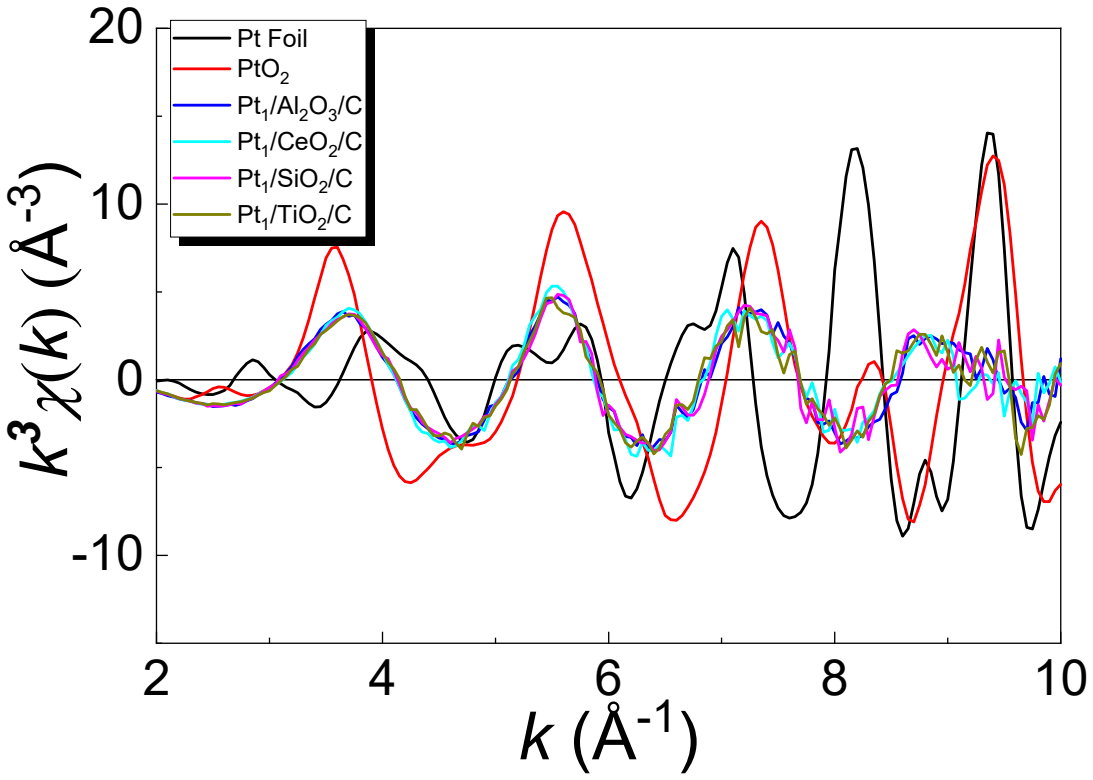

Figure S16 k^3-weighted FT-EXAFS spectra of Pt Foil, PtO_2, and Pt_1/oxide/C.

Figure S17

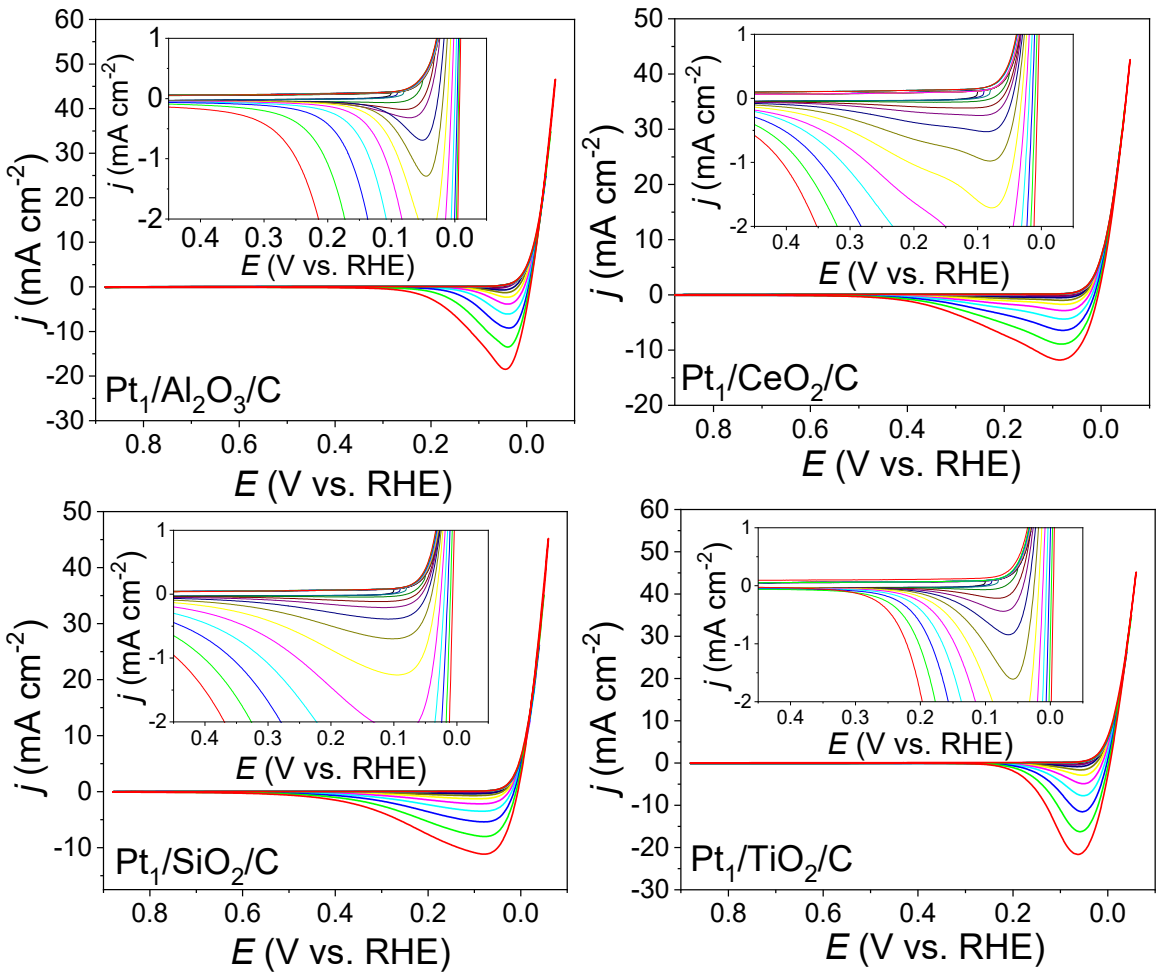

Figure S17 CVs of Pt_1/oxide/C recorded at various reversed potentials in Ar-saturated 0.5 M H_2SO_4 at a scan rate of 50 mVs^{-1}.

Figure S18

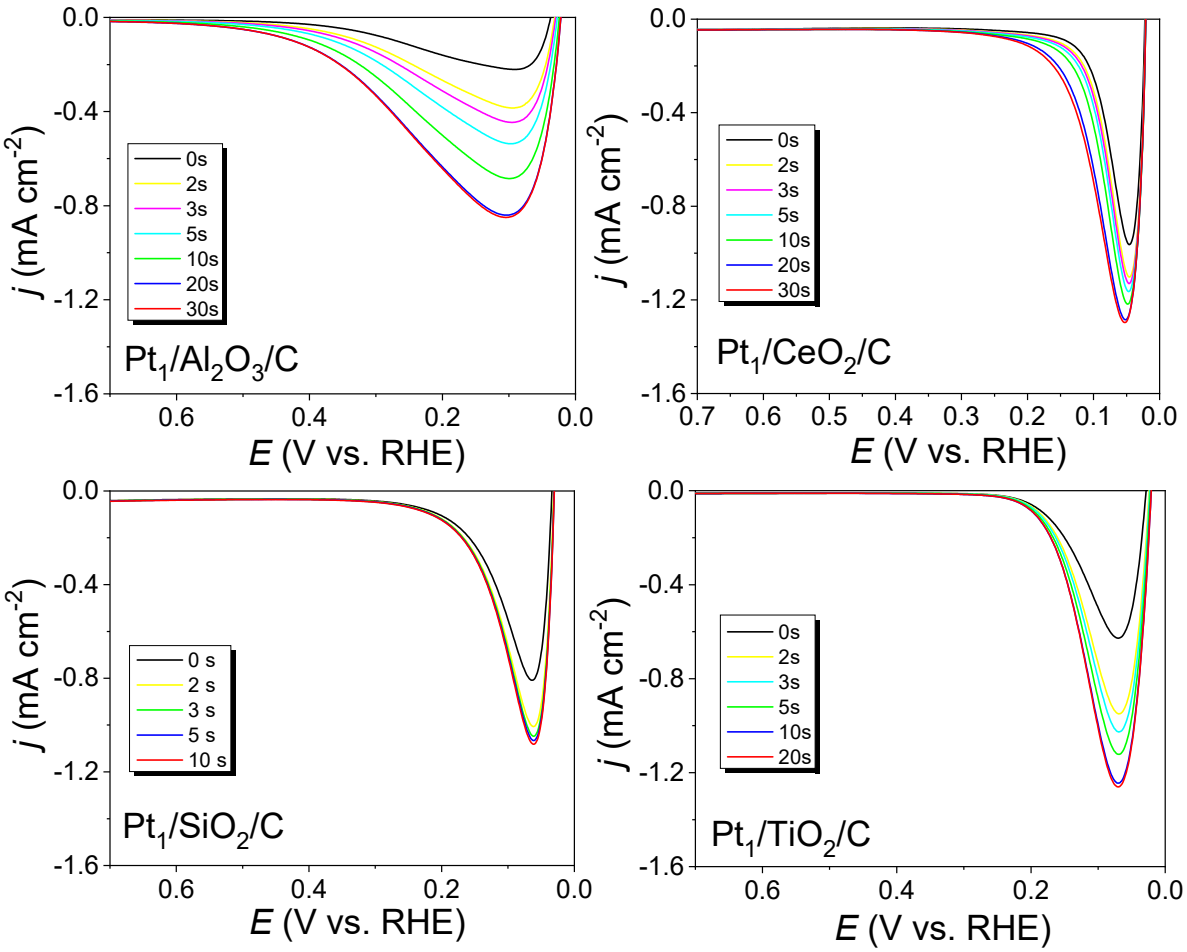

Figure S18 Anodic LSVs for H_{upd} recorded on Pt_1/oxide/C (0.19 μg cm^{-2} Pt loading) after holding at 0.04 V for various durations.

Figure S19

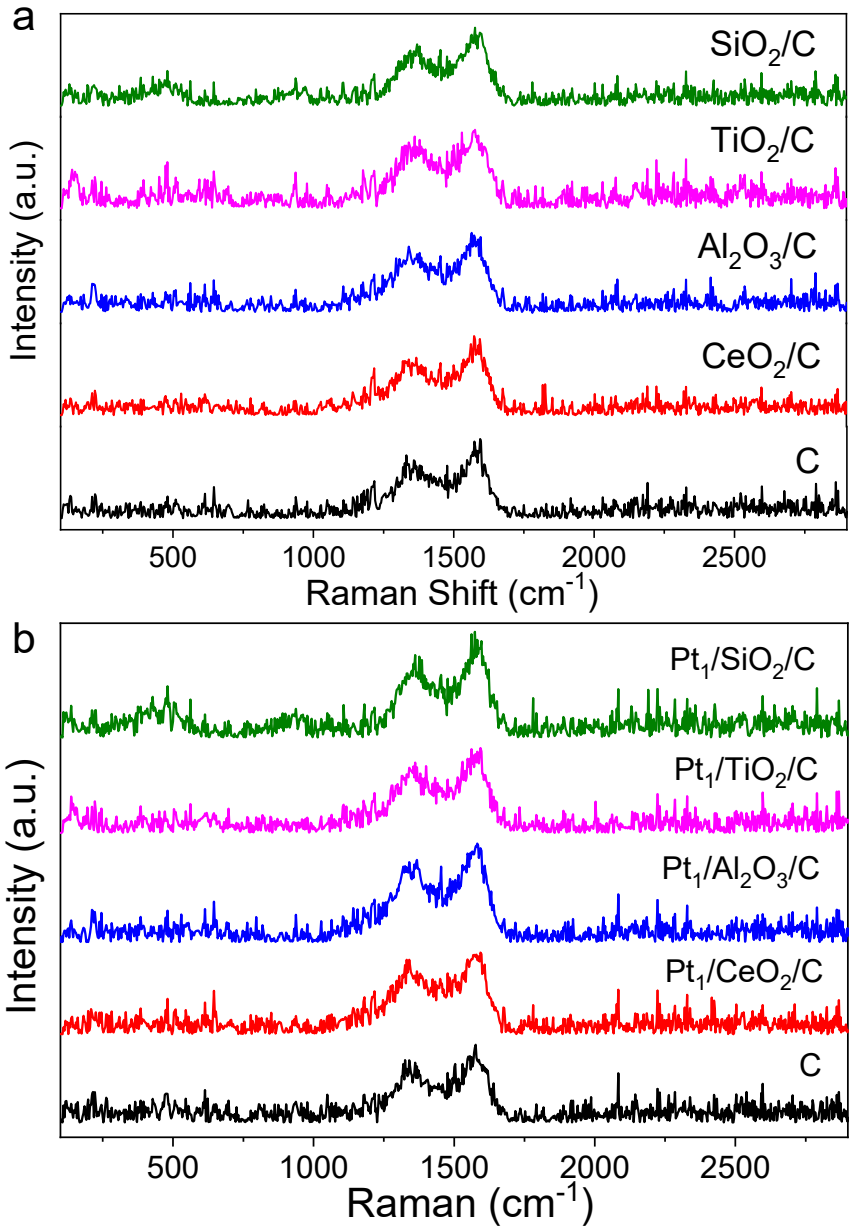

Figure S19 Raman spectra of C, (a) oxide/C, and (b) Pt_1/oxide/C

The Stability of Pt_1/oxide/C in the HER Process

To evaluate its durability, Pt_1/oxide/C underwent 2000 continuous potential cycles from 0.8 V to -0.1 V vs. RHE at a scan rate of 0.05 V/s. The polarization curves for the first and 2000th cycles remained almost identical, with no significant changes, as shown in Figs S20a-S20d. Although Pt ions may transfer into the electrolyte under high anodic potentials (>0.8 V vs. RHE), they remained stable under cathodic HER conditions. ICP-MS analysis confirmed that the Pt^{2+} content in the electrolyte was below 5 ppb, indicating that Pt_1 sites on Pt_1/oxide/C remained intact, and the catalyst did not deactivate during HER operation.

For practical application, the stability of Pt_1/oxide/C was further examined at a moderate current density (~35 mA cm^{-2}, corresponding to an overpotential of 50 mV. PS: the catalyst ink is unstable at large current density, ~100 mA cm^{-2}). Chronoamperometry (CA) measurements (Fig. S20e) showed that Pt_1/oxide/C retained 95% of its initial current after 1 hour. Although the current density gradually dropped to 85% in the first hour, it remained stable over 10 hours, with no significant increase in Pt^{2+} content in the electrolyte. However, CV tracking results revealed a slight cathodic shift in the HER onset potential from 0.05 V to 0.0 V vs. RHE, which is close to the behavior of bulk Pt. Since the Pt content in the catalyst did not significantly decrease, this activity decline is likely due to electrode surface polarization effects, causing Pt single-atom migration and aggregation into larger clusters during HER operation. This issue needs to be further addressed to enhance the long-term stability of Pt_1/oxide/C under high-current density HER conditions.

Figure S20

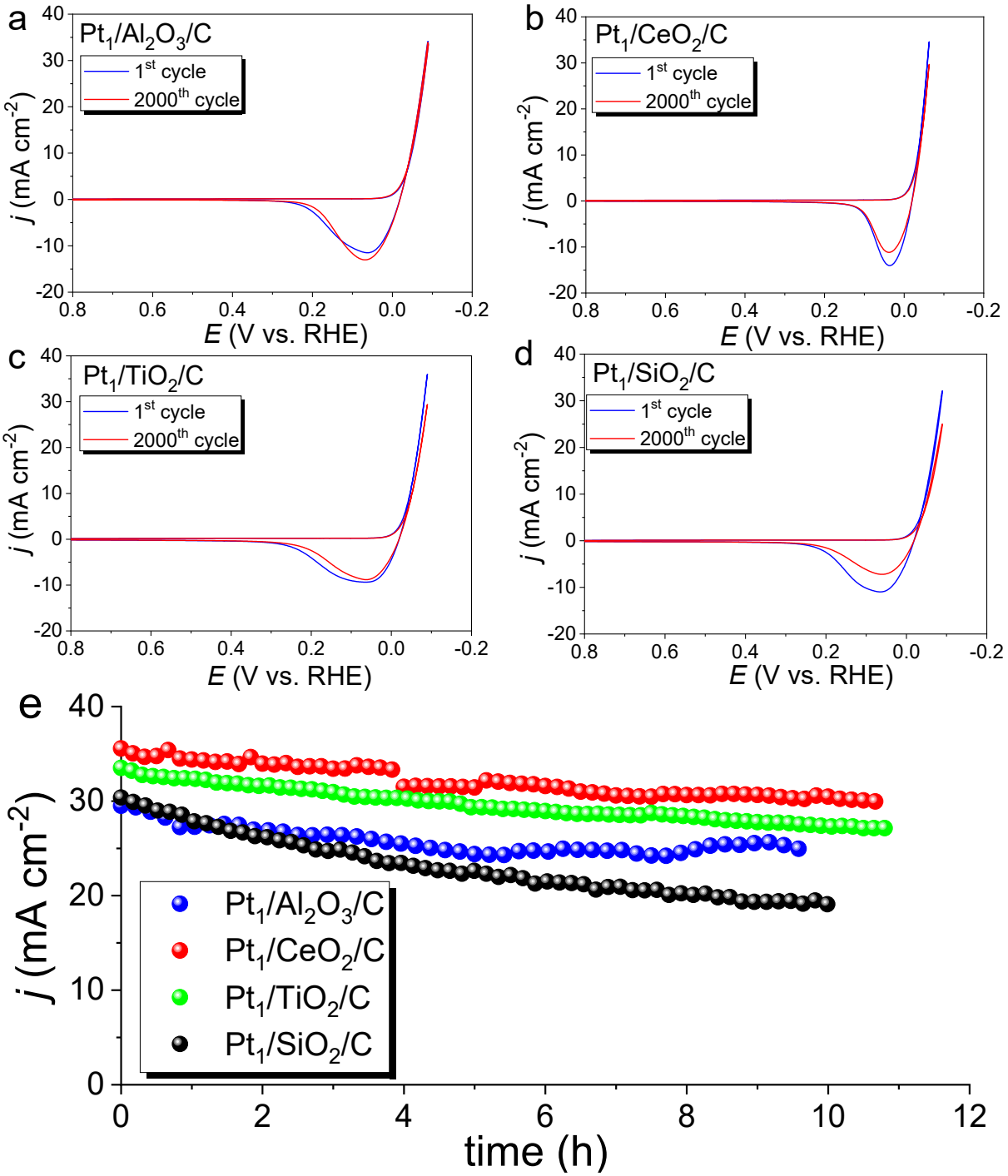

Figure S20. (a)(b)(c)(d) CVs of Pt_1/oxide/C were recorede at (blue line) the first and (red line) the 2000th cycles in 0.5 M H_2SO_{4aq}. (e) Long-term stability of Pt_1/oxide/C examined by chronoamperometry at overpotentials of 50 mV (current density ~35 mA cm^{-2}) for HER in 0.5 M H_2SO_{4aq}.

Table S1 The characteristics of Pt_1/oxide/C and Pt/C measured by electrochemical method

Catalyst	A_{BET}*	Q_{CO}	Q_{Hupd}	$sECSA_{CO}$*	$sECSA_H$*	d_{av}	N_{Pt1}/A_{BET}	D_{ee}
	m^2/g	μC	μC	m^2/g	m^2/g	nm	k μm^{-2}	nm
$Pt_1/Al_2O_3/C$	61.3	42.3	22.7	740.6	794.6	0.35±0.1	683.1±1.5	0.86±0.03
$Pt_1/CeO_2/C$	35.8	48.7	22.3	852.7	779.8	0.36±0.1	1105.2±2.2	0.59±0.02
$Pt_1/SiO_2/C$	43.2	43.2	22.2	756.3	777.3	0.36±0.1	907.6±2.0	0.69±0.02
$Pt_1/TiO_2/C$	47.3	42.6	22.2	746.2	778.2	0.36±0.1	831.0±3.2	0.74±0.04
Pt/C	124.9	2.96	1.21	52.9	57.5	4.86±0.3	0.094±0.006	98.6±0.2

* A_{BET}: the Brunauer-Emmett-Teller (BET) surface area of oxides or carbon; $sECSA_{CO}$ and $sECSA_H$: the specific ECSA of Pt (sECSA = ECSA/Pt weight, $m^2\ g^{-1}$) was evaluated from $ECSA_{CO}$ and $ECSA_H$.

Table S2. HER performances of Pt-SACs and Pt-catalysts

Catalysts	Tafel (mV/dec)	η_{10} (mV)	TOF (s^{-1})	$i_{mPt(\eta/mV)}$ (A/mg)	electrolyte	Refs.
$Pt_1/Al_2O_3/C$	32.1	16	490.1	484.8	0.5M H_2SO_4	This work
$Pt_1/CeO_2/C$	30.6	11	586.4	580.2	0.5M H_2SO_4	
$Pt_1/SiO_2/C$	31.1	12	503.5	498.2	0.5M H_2SO_4	
$Pt_1/TiO_2/C$	31.2	12	576.9	570.6	0.5M H_2SO_4	
Pt/C	32.1/121.6	71	1.9	1.9	0.5M H_2SO_4	
Pt−Ru dimer	26	59	4.14	3.49	0.5M H_2SO_4	s[1]
CoPt-Pt_{SA}/NDPCF	24.84	20	75.11_{50}	74.31_{50}	0.5M H_2SO_4	s[2]
Pt/N-VG-5	52.2	42	N/A	4.45_{50}	0.5M H_2SO_4	s[3]
P-Pt_3Co/NC	13	136	1.33	59.8	0.5M H_2SO_4	s[4]
Pt_1 SAC-VNGNMAs	49	15	$\sim1.5_{50}$	$\sim1.5_{50}$	0.5M H_2SO_4	s[5]
Pt/$TiON_x$	29.5	N/A	12.15_{50}	1.41_{50}	0.1 M $HClO_4$	s[6]
A-Pt	97.0	89.7	0.487_{10}	0.948_{10}	0.5M H_2SO_4	s[7]
$Ti_3C_2T_x$-PtSA	45	38	23.45	23.21	0.5M H_2SO_4	s[8]
PtW_6O_{24}/C	29.8	22	33.35_{100}	20.175_{77}	0.5M H_2SO_4	s[9]
$Pt_1^{O1}/Ti_{1-x}O_2$	31	22	N/A	23.92_{50}	0.5M H_2SO_4	s[10]
PtCo@PtSn	24	21	3.3	3.31	0.5M H_2SO_4	s[11]
Pt-PVP/TNR@GC	27	21	N/A	16.53_{50}	0.5M H_2SO_4	s[12]
AC Pt-NG/C	27	35.28	0.0927_{50}	6.508_{50}	0.5M H_2SO_4	s[13]
Pt/$RuCeO_x$-PA	31	41	N/A	0.375_{50}	0.5M H_2SO_4	s[14]
3Pt/CuG	27.6	20	N/A	40.1_{50}	0.5M H_2SO_4	s[15]
LPWGA	30	42	29.05_{50}	28.70_{50}	0.5M H_2SO_4	s[16]
2-Pt/NC-CC	36.65	123	0.9354_{50}	0.907_{50}	0.5M H_2SO_4	s[17]
Pt@DG	48	30	26.41_{100}	28.38_{100}	0.5M H_2SO_4	s[18]
Pt/NiO@Ni/NF	40	34	N/A	0.532_{50}	1M KOH	s[19]
Pt-SAs/C	43	38	N/A	3.01_{50}	0.5M H_2SO_4	s[20]
$Pt_{0.2}$-CeO_2	35	N/A	N/A	7.6_{50}	0.5M H_2SO_4	s[21]
Pt-SAs/MoS_2	28	32	12.83_{50}	47.48_{100}	0.5M H_2SO_4	s[22]
PtO_x/TiO_2	40	N/A	N/A	8.68_{50}	0.5M H_2SO_4	s[23]
Pt_2Ir DNWs/C	20.9	26	17.08_{50}	5.17_{50}	0.5M H_2SO_4	s[24]
Pt/MXene	297	34	10.66	1.847_{50}	0.5M H_2SO_4	s[25]
Pt-SAs/EVG	35	21.3	34.60_{70}	32.90_{70}	0.5M H_2SO_4	s[26]

NGA-COF@Pt	21.88	13	18.40_{44}	18.165_{44}	0.5M H_2SO_4	s[27]
Pt_1+Pt_n/MXene-7	32.5	61.3	0.488_{100}	0.4849_{100}	0.5M H_2SO_4	s[28]
PtSA-M-CeO_2-X/rGO	22.8	25	15.46_{50}	15.3_{50}	0.5M H_2SO_4	s[29]
Pt-SA/pCNFs	24	21	14.8_{50}	$\sim 14_{50}$	0.5M H_2SO_4	s[30]
Pt@Mn-SAs/N-C	30.7	25	N/A	1.5_{50}	0.5M H_2SO_4	s[31]
Pt_1Ru_x@C	20.7	13.15	N/A	9.075_{100}	0.5M H_2SO_4	s[32]
Pt/V・-Mn_3O_4 NSs	30.2	19.2	44.54_{100}	12.56_{50}	0.5M H_2SO_4	s[33]

Table S3. The best-fiting FT-EXAFS parameters of Pt_1/oxide/C catalysts*

	Scattering Path	N	σ^2 (Å^2)	R(Å)	R_f
Pt foil	Pt-Pt	12	0.005	2.76	0.002
PtO_2	Pt-O	6	0.003	2.02	0.006
$Pt_1/Al_2O_3/C$	Pt-O	3.6	0.003	2.09	0.005
$Pt_1/CeO_2/C$	Pt-O	3.8	0.002	2.1	0.004
$Pt_1/SiO_2/C$	Pt-O	3.6	0.003	2.11	0.016
$Pt_1/TiO_2/C$	Pt-O	3.7	0.004	2.11	0.01

*Where N is coordination number, R is distance between absorber and backscatter atoms, σ^2 is Debye–Waller factor value, R_f is R-factor characterizing the goodness of fit. S_o^2 was fixed to 0.8 as determined from PtO_2 fitting. Error bounds (accuracies) characterizing the structural parameters obtained by EXAFS data analysis are estimated to be as follows: N, ±20%; R, ±1%; and σ^2, ±20%.

Author Contributions

Conceptualization: JFH

Methodology and experiment: JFH, LJC, BZY, JLC

Investigation: JFH, LJC, BZY, JLC

Funding acquisition: JFH

Project administration: JFH

Supervision: JFH

Writing: JFH

References

S1. W. K. Zhao, C. Luo, Y. Lin, G. B. Wang, H. M. Chen, P. Y. Kuang and J. G. Yu, *ACS Catal.*, 2022, **12**, 5540-5548.

S2. W. W. Yang, P. Cheng, Z. Li, Y. X. Lin, M. Y. Li, J. Z. Zi, H. H. Shi, G. S. Li, Z. C. Lian and H. X. Li, *Adv. Funct. Mater.*, 2022, **32**, 2205920.

S3. H. Z. Yang, Z. J. Yang, Z. J. Han, D. W. Chu, C. Q. Chen, X. Y. Xie, L. Shang and T. R. Zhang, *2D Mater.*, 2022, **9**, 045011.

S4. C. F. Li, C. Tian, H. B. Tang, M. R. Liu, L. R. Zheng, F. Z. Huang, G. R. Li and Q. Li, *ACS Energy Lett.*, 2023, **8**, 5161-5169.

S5. K. Chi, Z. X. Chen, F. Xiao, W. Guo, W. Xi, J. Liu, H. Yan, Z. Y. Zhang, J. Xiao, J. Liu, J. Luo, S. Wang and K. P. Loh, *J. Mater. Chem. A*, 2019, **7**, 15575-15579.

S6. M. Smiljanic, S. Panic, M. Bele, F. Ruiz-Zepeda, L. Pavko, L. Gasparic, A. Kokalj, M. Gaberscek and N. Hodnik, *ACS Catal.*, 2022, **12**, 13021-13033.

S7. Z. H. Ma, C. Chen, X. Z. Cui, L. M. Zeng, L. J. Wang, W. Jiang and J. L. Shi, *ACS Appl. Mater. Interfaces*, 2021, **13**, 44224-44233.

S8. J. J. Zhang, E. Q. Wang, S. Q. Cui, S. B. Yang, X. L. Zou and Y. J. Gong, *Nano Lett.*, 2022, **22**, 1398-1405.

S9. F. Y. Yu, Z. L. Lang, L. Y. Yin, K. Feng, Y. J. Xia, H. Q. Tan, H. T. Zhu, J. Zhong, Z. H. Kang and Y. G. Li, *Nat. Commun.*, 2020, **11**, 490.

S10. F. Lu, D. Yi, S. J. Liu, F. Zhan, B. Zhou, L. Gu, D. Golberg, X. Wang and J. N. Yao, *Angew. Chem. Int. Ed.*, 2020, **59**, 17712-17718.

S11. J. L. Chen, G. F. Qian, H. Zhang, S. Q. Feng, Y. S. Mo, L. Luo and S. B. Yin, *Adv. Funct. Mater.*, 2022, **32**, 2107597.

S12. C. Li, Z. Chen, H. Yi, Y. Cao, L. Du, Y. D. Hu, F. P. Kong, R. K. Campen, Y. Z. Gao, C. Y. Du, G. P. Yin, I. Y. Zhang and Y. J. Tong, *Angew. Chem. Int. Ed.*, 2020, **59**, 15902-15907.

S13. M. H. Sun, J. P. Ji, M. Y. Hu, M. Y. Weng, Y. P. Zhang, H. S. Yu, J. J. Tang, J. C. Zheng, Z. Jiang, F. Pan, C. D. Liang and Z. Lin, *ACS Catal.*, 2019, **9**, 8213-8223.

S14. T. T. Liu, W. B. Gao, Q. Q. Wang, M. L. Dou, Z. P. Zhang and F. Wang, *Angew. Chem. Int. Ed.*, 2020, **59**, 20423-20427.

S15. Y. D. Xu, D. M. Meng, L. W. Wang, H. Yang, X. F. Guo, Y. Zhu, T. Wang and W. P. Ding, *Appl. Surf. Sci.*, 2022, **591**, 153057.

S16. Y. Li, K. Y. Jiang, J. Yang, Y. Y. Zheng, R. Hübner, Z. W. Ou, X. Dong, L. Q. He, H. L. Wang, J. Li, Y. J. Sun, X. B. Lu, X. D. Zhuang, Z. K. Zheng and W. Liu, *Small*, 2021, **17**, 2102159.

S17. R. Ramesh, S. Han, D. K. Nandi, S. Y. Sawant, D. H. Kim, T. Cheon, M. H. Cho, R. Harada, T. Shigetomi, K. Suzuki and S. H. Kim, *Adv. Mater. Interfaces*, 2021, **8**, 2001508.

S18. Q. Yang, H. X. Liu, P. Yuan, Y. Jia, L. Z. Zhuang, H. W. Zhang, X. C. Yan, G. H. Liu, Y. F. Zhao, J. Z. Liu, S. Q. Wei, L. Song, Q. L. Wu, B. Q. Ge, L. Z. Zhang, K. Wang, X. Wang, C. R. Chang and X. D. Yao, *J. Am. Chem. Soc.*, 2022, **144**, 2171-2178.

S19. Z. J. Chen, G. X. Cao, L. Y. Gan, H. Dai, N. Xu, M. J. Zang, H. B. Dai, H. Wu and P. Wang, *ACS Catal.*, 2018, **8**, 8866-8872.

S20. Z. Y. Wang, J. Yang, J. Gan, W. X. Chen, F. Y. Zhou, X. Zhou, Z. Q. Yu, J. F. Zhu, X. Z. Duan and Y. E. Wu, *J. Mater. Chem. A*, 2020, **8**, 10755-10760.

S21. J. J. Gao, P. Du, Q. H. Zhang, X. Shen, F. K. Chiang, Y. R. Wen, X. Lin, X. J. Liu and H. J. Qiu, *Electrochim. Acta*, 2019, **297**, 155-162.

S22. Y. Shi, Z. R. Ma, Y. Y. Xiao, Y. C. Yin, W. M. Huang, Z. C. Huang, Y. Z. Zheng, F. Y. Mu, R. Huang, G. Y. Shi, Y. Y. Sun, X. H. Xia and W. Chen, *Nat. Commun.*, 2021, **12**, 3021.

S23. X. Cheng, Y. H. Li, L. R. Zheng, Y. Yan, Y. F. Zhang, G. Chen, S. R. Sun and J. J. Zhang, *Energy Environ. Sci.*, 2017, **10**, 2450-2458.

S24. M. M. Wang, M. J. Wang, C. H. Zhan, H. B. Geng, Y. H. Li, X. Q. Huang and L. Z. Bu, *J. Mater. Chem. A*, 2022, **10**, 18972-18977.

S25. Y. C. Wu, W. Wei, R. H. Yu, L. X. Xia, X. F. Hong, J. X. Zhu, J. T. Li, L. Lv, W. Chen, Y. Zhao, L. Zhou and L. Q. Mai, *Adv. Funct. Mater.*, 2022, **32**, 2110910.

S26. B. W. Ren, J. D. Huang, P. Li, W. Xu and B. Dong, *J. Colloid Interface Sci.*, 2025, **678**, 511-519.

S27. Z. Q. Zhang, Z. Zhang, C. L. Chen, R. Wang, M. G. Xie, S. Wan, R. G. Zhang, L. C. Cong, H. Y. Lu, Y. Han, W. Xing, Z. Shi and S. H. Feng, *Nat. Commun.*, 2024, **15**, s41467-41024-46872-x.

S28. X. Sun, J. Wang, J. Yu, Y. F. Jing, J. Y. Liu, M. Singh, P. D. Lund and M. I. Asghar, *Int. J. Hydrog. Energy*, 2024, **84**, 502-510.

S29. X. Y. Liu, Y. X. Zhou, J. K. Lin, X. Xiao, Z. J. Wang, L. Y. Jia, M. Y. Li, K. Yang, J. C. Fan, W. W. Yang and G. S. Li, *Angew. Chem.-Int. Edit.*, 2024, **63**, anie202406650.

S30. Y. Han, H. L. Duan, W. Liu, C. H. Zhou, B. S. Wang, Q. Y. Jiang, S. H. Feng, W. S. Yan, T. Tan and R. F. Zhang, *Appl. Catal. B-Environ. Energy*, 2023, **335**, 9.

S31. L. Gong, J. W. Zhu, F. J. Xia, Y. H. Zhang, W. J. Shi, L. Chen, J. Yu, J. S. Wu and S. C. Mu, *ACS Catal.*, 2023, **13**, 4012-4020.

S32. X. Y. Zhu, M. H. Fang, B. Z. Yang, M. L. Zhan, S. R. Ke, F. Yang, X. W. Wu, Y. G. Liu, Z. H. Huang and X. Min, *J. Mater. Chem. A*, 2024, **12**, 4108-4122.

S33. D. X. Hu, Y. J. Wang, W. H. Chen, Z. Q. Jiang, B. L. Deng and Z. J. Jiang, *Small*, 2024, DOI: 10.1002/smll.202402652.